The influence of surface structure on the catalytic activity of cerium promoted copper oxide catalysts on alumina: oxidation of carbon monoxide and methane

Paul Worn Park * and Jeffrey S. Ledford ‡

Department of Chemistry, The Center for Fundamental Materials Research, Michigan State University, East Lansing, MI 48824-1322, USA

Received 11 July 1997; accepted 17 November 1997

X-ray diffraction (XRD) and X-ray photoelectron spectroscopy (XPS) have been used to characterize a series of $Cu/Ce/Al_2O_3$ catalysts. Catalysts were prepared by incipient wetness impregnation using metal nitrate and alkoxide precursors. Catalyst loadings were held constant at 12 wt% CuO and 5.1 wt% CeO_2. Mixed oxide catalysts were prepared by impregnation of cerium first, followed by copper. The information obtained from surface and bulk characterization has been correlated with CO and CH_4 oxidation activity of the catalysts. Cu/Al_2O_3 catalysts prepared using Cu(II) nitrate (CuN) and Cu(II) ethoxide (CuA) precursors consist of a mixture of copper surface phase and crystalline CuO. The CuA catalyst shows higher dispersion, less crystalline CuO phase, and lower oxidation activity for CO and CH_4 than the CuN catalyst. For $Cu/Ce/Al_2O_3$ catalysts, Ce has little effect on the dispersion and crystallinity of the copper species. However, Cu impregnation decreases the Ce dispersion and increases the amount of crystalline CeO_2 present in the catalysts, particularly in Ce modified alumina prepared using cerium alkoxide precursor (CeA). Cerium addition dramatically increases the CO oxidation activity, however, it has little effect on CH_4 oxidation.

Keywords: CuO, CeO_2, Al_2O_3, CO oxidation, CH_4 oxidation, XPS, XRD

1. Introduction

Copper oxide is a well known component of catalysts for CO [1–6], hydrocarbon [1–3,7], chlorinated hydrocarbon [8] and alcohol oxidation [9,10] as well as for NO_x [11–13] and SO_2 reduction [13]. These air purification reactions using heterogeneous catalysts have been important topics due to their application to automobile exhaust converters and industrial waste incinerators. Copper oxide based catalysts have been considered as suitable substitutes for noble metal catalysts in emission control applications due to their high catalytic activity for the purification reactions, tolerance to SO_2 [3] and refractory nature [14]. Several researchers reported that copper oxide based catalysts show similar activity to noble metal catalysts for CO oxidation [2], butanal and mercaptan oxidation [15], and reduction of NO by CO [13].

Rare earth oxide additives have been widely applied as textural and structural promoters for supported noble metal catalysts. Cerium addition prevents γ-alumina from sintering at high temperature and improves the dispersion and thermal stability of noble metals [16–20]. In addition, cerium oxide has been added to noble metal catalysts for treatment of automobile exhaust to promote the water–gas shift reaction [21,22], to suppress the CO inhibition effect [23–25], and to remove CO, hydrocarbons, and NO_x simultaneously using its oxygen storage ability [17,18,26–29].

Previous studies of rare earth promoters have focused primarily on their effects on the structure and activity of noble metal based catalysts. Study of the promoter effect on supported transition metal oxide catalysts has been relatively limited. Recently cerium oxide has been examined both as a promoter [30] and as a support [31] for oxidation reactions over copper oxide based catalysts. Agarwal et al. [30] found that a ceria promoted hopcalite catalyst has a higher initial activity for hydrocarbon oxidation than a Pt catalyst. Bedford and LaBarge [31] showed that copper–chromium oxide impregnated on high surface area ceria has three-way catalyst behavior and retains catalyst activity after aging at high temperature. Flytzani-Stephanopoulos and coworkers [32–34] reported recently that a Cu–Ce–O composite catalyst shows high activity for CO and CH_4 oxidation and high resistance to water poisoning. They attributed the enhanced catalytic activity and stability to the strong interaction of copper and cerium oxides. The effect of a CeO_2 promoter on alumina supported copper oxide catalysts has been reported to be similar to the effect it has on noble metal catalysts [35,36]. The authors suggested that the addition of CeO_2 enhances redox behavior of the copper ion, increases dispersion of the copper oxides, provides surface oxygen, and improves the oxygen storage capacity of catalyst.

While, cerium oxide promoted copper oxide based

* Current address: Center for Catalysis and Surface Science, Northwestern University, Evanston, IL 60208, USA.

‡ To whom correspondence should be addressed. Current address: Mobil Chemical Company, Films Division-Technical Center, 729 Pittsford-Palmyra Road, Macedon, NY 14502, USA.

catalysts have recently drawn the attention of many researchers, the effect of cerium oxide on the surface structure and reactivity of copper catalysts has not been studied extensively. The present work is part of a broad study to investigate structure–reactivity correlations for rare earth oxide promoted transition metal oxide based emission control catalysts. In this paper, X-ray photoelectron spectroscopy (XPS) and X-ray diffraction (XRD) have been used to determine the effect of catalyst precursors and cerium promotion on the chemical state and dispersion of copper oxide phases in a series of $Cu/Ce/Al_2O_3$ catalysts. The information derived from these techniques is correlated with CO and CH_4 oxidation activity to develop a more complete understanding of $Cu/Ce/Al_2O_3$ catalysts.

2. Experimental

2.1. Catalyst preparation

Catalysts were prepared by pore volume impregnation of γ-alumina (Cyanamid, surface area = 203 m^2/g, pore volume = 0.6 ml/g). The alumina was finely ground (< 230 mesh) and calcined in air at 500°C for 24 h prior to impregnation. Ce/Al_2O_3 catalysts were prepared using a deionized water solution of ammonium cerium(IV) nitrate (Mallinckrodt Inc., Analytical Reagent) or an ethanol solution of cerium(IV) methoxyethoxide (Gelest Inc., 18–20% cerium methoxyethoxide in methoxyethanol). The impregnated sample derived from the cerium nitrate solution (designated "CeN") was dried in air at 120°C for 24 h and calcined in air at 500°C for 16 h. The sample prepared using the cerium methoxyethoxide solution (designated "CeA") was impregnated and subsequently dried at room temperature for 48 h in a N_2 purged glove bag prior to further drying in air at 120°C for 24 h and calcination in air at 500°C for 16 h. The Ce loading was held constant at 5.1 wt% CeO_2. Cu/Al_2O_3 catalysts were prepared with a deionized water solution of copper(II) nitrate (Columbus Chemical Industries Inc, ACS Grade) or an aqueous diethylenetriamine solution (DETA/water ratio = 1/3 by volume) of copper(II) ethoxide. DETA addition was necessary due to the limited solubility of copper(II) ethoxide in water and common organic solvents. Since an aqueous DETA solution was used to dissolve copper(II) ethoxide, a Cu–DETA complex should be formed in the impregnating solution [37]. The impregnated samples derived from the aqueous copper nitrate solution (designated "CuN") and catalysts prepared with the aqueous DETA copper ethoxide solution (designated "CuA") were dried and calcined under the same conditions as used for CeN and CeA samples, respectively. The Cu loading was held constant at 12 wt% CuO. Mixed metal oxide catalysts were prepared by step-wise impregnation of Ce first, followed by Cu. The cerium modified alumina carrier was dried and calcined prior to introduction of copper. After the addition of copper, the catalysts were dried and calcined at the same conditions described above depending on the choice of precursors. Catalysts prepared using nitrate and alkoxide precursors will be symbolized using "N" and "A", respectively.

2.2. Standard materials

CuO and CeO_2 were prepared by calcining copper(II) nitrate and ammonium cerium(IV) nitrate in air at 500°C for 16 h. $CuAl_2O_4$ was prepared by calcining stoichiometric amounts of the respective nitrates in air at 1000°C for 24 h. $CeAlO_3$ was prepared by reduction of a dried CeA sample at 800°C in H_2 (AGA, 99.99%) for 8 h. XRD patterns of the standard compounds matched the appropriate Powder Diffraction File [38].

2.3. BET surface area

Surface area measurements were performed using a QuantaChrome Quantasorb Jr. Sorption System. Approximately 0.1 g of catalysts were outgassed in a N_2/He mixture (5% N_2) at 350°C for 1 h prior to adsorption measurements. The measurements were made using relative pressures of N_2 to He of 0.05, 0.08, and 0.15 (N_2 surface area = 0.162 nm^2) at 77 K. The addition of copper and/or cerium to the alumina carrier decreased the BET surface area by a maximum of 20%.

2.4. X-ray diffraction

X-ray powder diffraction patterns were obtained with a Rigaku XRD diffractometer employing Cu Kα radiation (λ = 1.5418 Å). The X-ray was operated at 45 kV and 100 mA. Diffraction patterns were obtained using a scanning rate of 0.5 deg/min (in 2θ) with divergence slit and scatter slit widths of 1°. Samples were run as powders packed into a glass sample holder having a $20 \times 16 \times 0.5$ mm cavity.

The mean crystallite sizes ($\bar{d}$) of the CuO and CeO_2 particles were determined from XRD line broadening measurements using the Scherrer equation [39]:

$$\bar{d} = K\lambda/\beta\cos\theta, \quad (1)$$

where λ is the X-ray wavelength, K is the particle shape factor, taken as 0.9, and β is the full width at half maximum (fwhm), in radians, of the CuO $\langle\bar{1}11\rangle$ or $CeO_2\langle111\rangle$ line.

Quantitative X-ray diffraction data were obtained by comparing $CuO\langle\bar{1}11\rangle/Al_2O_3\langle400\rangle$ or $CeO_2\langle111\rangle/Al_2O_3\langle440\rangle$ intensity ratios measured for catalyst samples with intensity ratios measured for physical mixtures of pure CuO or CeO_2 and γ-Al_2O_3. This method assumed that copper or cerium addition did not disrupt the γ-Al_2O_3 spinel and subsequently affect the intensity

of the Al_2O_3 ⟨400⟩ line. The error in this method was estimated to be ±20%.

2.5. XPS analysis

XPS data were obtained using a Perkin-Elmer Surface Science instrument equipped with a magnesium anode (1253.6 eV) operated at 300 W (15 kV, 20 mA) and a 10-360 hemispherical analyzer operated with a pass energy of 50 eV. The instrument typically operates at pressures near 1×10^{-8} Torr in the analysis chamber. Spectra were collected using a PC137 board interfaced to a Zeos 386SX computer. Samples were analyzed as powders dusted onto double-sided sticky tape or spray coated onto a quartz slide using a methanol suspension of the catalyst. Binding energies for the catalyst samples and standard compounds which contained Al were referenced to the Al 2p peak (74.5 eV). The binding energies for standard compounds that did not contain Al were referenced to the C 1s line (284.6 eV) of the carbon overlayer. XPS binding energies were measured with a precision of ±0.2 eV, or better.

Reduction of copper [40–42] and cerium [43–46] species during XPS experiments has been reported and attributed to several factors such as X-ray flux, X-ray dose, temperature, and pressure. In order to minimize the effect of photoreduction on the results, all samples were analyzed using the same distance between X-ray source and sample (2 cm) and minimum data acquisition time (5 min scan for Cu $2p_{3/2}$ spectra). No significant photoreduction of copper species was observed using these experimental conditions. However, in order to obtain reasonable quality spectra, the Ce 3d region must be scanned for an extended time (∼ 600 min). We have previously reported [46] that extended scan times lead to photoreduction of supported cerium oxides. Ce XPS data were used only to measure Ce dispersion on alumina.

2.6. Quantitative XPS analysis

It has been shown by Defosse et al. [47] that one may calculate the theoretical intensity ratio I_p^0/I_s^0 expected for a supported phase (p) atomically dispersed on a carrier (s). An extension of the Defosse model proposed by Kerkhof and Moulijn [48] has been used in the present investigation. The photoelectron cross sections and the mean escape depths of the photoelectrons used in these calculations were taken from Scofield [49] and Penn [50], respectively. For a phase (p) present as discrete particles, the experimental intensity ratio I_p/I_s is given by the following expression:

$$I_p/I_s = I_p^0/I_s^0[1 - \exp(-d/\lambda_p)]/(d/\lambda_p)\,, \qquad (2)$$

where I_p^0/I_s^0 is the theoretical monolayer intensity ratio, d is the length of the edge of the cubic crystallites of the deposited phase and λ_p is the mean escape depth of the photoelectrons in the deposited phase. Particle sizes of the Cu or Ce species were determined by solving eq. (2). The relative Cu or Ce dispersion was estimated from the ratio of I_p/I_s to I_p^0/I_s^0.

2.7. CO oxidation activity

CO oxidation activity measurements were performed in a flow microreactor. Approximately 0.03 g of catalyst were supported on a glass frit (70–100 μm) and the temperature was measured with a K-type thermocouple located just above the catalyst bed. The reactor was heated by a tube furnace (Lindberg) with temperature being controlled within 1°C by an Omega CN 1200 temperature controller. Reactant gas flow rates were held constant with Brooks 5850 mass flow controllers. Product gases were analyzed with a Varian 920 gas chromatograph equipped with a TCD and interfaced to a Hewlett-Packard 3394A integrator. Reaction products were separated on a 6 ft 60/80 mesh Carbosieve S-II column. Prior to the first activity measurement, catalysts were pretreated with a mixture of 5% O_2/He (99.5% purity for O_2, 99.995% purity for He, AGA Gas Co.) stream (143 cm^3/min) at 350°C for 1 h to remove any impurities absorbed on the surface of the catalyst during preparation and storage. CO oxidation reactions were performed with a constant flow rate (80 cm^3/min) of 4.8% CO/9.8% O_2/85.4% He gas mixture (AGA, purity > 99.99%) in the temperature range of 100–220°C.

2.8. CH_4 oxidation activity

Methane oxidation reactions were performed with a constant flow (15 cm^3/min) of 0.98% CH_4/5.25% O_2/93.77% He gas mixture (AGA, purity > 99.99%) in the temperature range of 360–420°C. Approximately 0.1 g catalyst were charged into the same type of microreactor used for CO oxidation measurements. Water produced during methane oxidation was frozen downstream from the reactor in a trap maintained at < −40°C with a mixture of ethanol and dry ice. No partial oxidation product was observed. All activity measurements (CO and CH_4 oxidation) were obtained under steady-state conditions at conversions less than 15%. Turnover frequency (TOF) was calculated using CO and CH_4 oxidation rates at 160 and 390°C, respectively, normalized by surface copper atoms determined from Cu content and dispersion.

3. Results and discussion

3.1. Chemical state and dispersion of cerium/alumina catalysts

The chemical state and dispersion of cerium oxide in cerium modified alumina (CeN and CeA) have been

reported previously [46]. In summary, for the CeA, only 0.3 wt% crystalline CeO_2 was detected by XRD (table 1, figure 1b), indicating that most of the cerium oxide is present as an amorphous phase. A large amount of crystalline CeO_2 (4.6 wt%) was observed for CeN (table 1, figure 1c), although a low cerium loading (5.1 wt%) and high surface area alumina support (203 m^2/g) were used in this study. The Ce dispersion determined by XPS results was found to be poor in both catalysts (table 2). Le Normand et al. [20] and Shyu et al. [51] have reported that for cerium catalysts with < 2.6 μmol ceria/m^2 alumina (< 9 wt% CeO_2/200 m^2 Al_2O_3), Ce species were present as $CeAlO_3$ dispersed surface phase and/or as small CeO_2 crystallites which were not detectable by XRD. The inconsistency between our work and that of previous researchers can be readily understood when one considers that the cerium precursor used in this study (Ce^{4+}) was different from the one used in others (Ce^{3+}). The Ce^{4+} precursor cannot occupy cation vacancies or substitute isomorphously for Al^{3+} in the alumina lattice because Ce^{4+} does not have the same oxidation state as Al^{3+}. This limits the interaction of Ce^{4+} and the alumina support, which leads to the formation of CeO_2 during sample preparation.

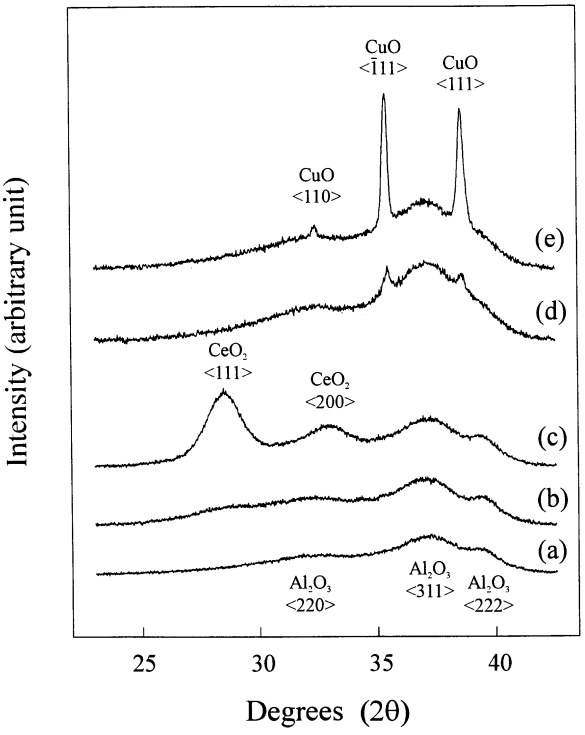

Figure 1. XRD patterns measured for (a) alumina support and (b) CeA, (c) CeN, (d) CuA, and (e) CuN catalysts.

3.2. Chemical state of copper/alumina catalysts

The XRD patterns obtained for CuA and CuN catalysts are shown in figures 1d and 1e. The XRD pattern of the CuN catalyst shows intense peaks characteristic of CuO, however, weak CuO lines are observed in the diffraction pattern of the CuA catalyst. Quantitative XRD measurements indicate that the CuN catalyst contains 5.5 wt% crystalline CuO phase, while the CuA catalyst contains only 0.8 wt% crystalline CuO (table 1). For alumina supports with surface area comparable to that used in this study, previous results [40,52] suggest that up to 8 wt% Cu can be incorporated into the alumina lattice as a Cu–Al_2O_3 surface phase when copper nitrate precursor is used to prepare the catalyst. Our finding that 6.5 wt% of the copper oxide is present as a dispersed phase for the CuN catalyst is in good agreement with previous work. In addition, the XPS Cu $2p_{3/2}$ binding energies measured for CuN and CuA catalysts (935.1 eV) are consistent with the value measured for $CuAl_2O_4$ (935.0 eV) and higher than the value measured for CuO (933.9 eV). Thus, XRD and XPS results suggest that copper is present predominantly as a copper surface phase on the alumina support.

3.3. Dispersion of copper/alumina catalysts

Particle sizes determined for CuN and CuA catalysts using XRD line broadening calculations and XPS Cu/

Table 1
Concentration of crystalline [a] phases in Cu/Ce/Al_2O_3 catalysts calculated from quantitative XRD data

Catalyst	Crystalline phase (wt%)	
	CeO_2	CuO
CeN	4.6	–[b]
CeA	0.3	–[b]
CuN	–[b]	5.5
CuA	–[b]	0.8
CuNCeN	4.7	6.0
CuACeN	4.1	0.6
CuNCeA	3.4	5.5
CuACeA	1.5	0.8

[a] Valid for crystalline phases with particle sizes > 3.0 nm.
[b] Catalysts do not contain the component.

Table 2
Particle size of cerium and copper phases determined from XRD line broadening calculations and XPS intensity ratios

Catalyst	Particle size (nm)			
	cerium		copper	
	XRD	XPS	XRD	XPS
CeN	5.1	1.6	–[a]	–[a]
CeA	4.5	1.6	–[a]	–[a]
CuN	–[a]	–[a]	30	1.9
CuA	–[a]	–[a]	30	1.1
CuNCeN	5.1	3.0	32	2.1
CuACeN	5.4	3.6	32	1.1
CuNCeA	4.1	4.1	32	2.2
CuACeA	4.6	4.7	30	1.1

[a] Catalysts do not contain the component.

Al intensity ratios are shown in table 2. CuO particle sizes determined using XRD line broadening calculations are identical for CuN and CuA catalysts. However, the copper species particle size determined for the CuA catalyst using XPS is smaller than the value obtained for the CuN catalyst. XPS and XRD analyses of the CuA catalyst indicate the formation of less crystalline and more dispersed copper species on the alumina support compared to CuN catalyst. From quantitative XRD data, approximately 11.2 wt% CuO in CuA is not detected by XRD can be assigned as a dispersed copper species on the alumina surface. However, the relatively poor Cu dispersion compared to monolayer noted for CuA catalyst indicates that it is not entirely due to a Cu–Al_2O_3 surface phase, since copper surface phase is normally considered to be highly dispersed. These results suggest that a dispersed amorphous copper oxide phase is formed on the CuA catalyst. Uchikawa and Mackenzie [37] have proposed that a polymeric gel was obtained after a solution of copper ethoxide–aqueous DETA was heated at 90°C. Therefore, the polymer structure is possibly obtained during the drying of aqueous copper ethoxide–DETA solution and then an amorphous CuO phase may be formed subsequently in the calcination step. It is also possible that Cu–DETA complexes aggregate less during catalyst preparation than the copper nitrate precursor.

The CuO particle sizes of all copper catalysts determined with XRD are significantly larger than the values obtained from XPS (table 2). This difference may be attributed to the limitations of X-ray diffraction. It is well known that XRD determined particle sizes are skewed to large values since XRD does not detect highly dispersed species. For the copper catalysts, a significant fraction of the Cu is present as a copper surface phase or small CuO particles ($d < 3.0$ nm) that are detected by XPS but not by XRD. Thus, smaller average particle sizes are expected from XPS calculations.

3.4. Chemical state of copper/cerium/alumina catalysts

Figure 2 shows the XRD patterns obtained for Cu/Ce/Al_2O_3 catalysts. The XRD patterns show only peaks characteristic of CuO and CeO_2. This is consistent with studies which have found that copper oxide is immiscible with cerium oxide [33]. For the Cu/Ce/Al_2O_3 catalysts prepared using CeN support (i.e. CuNCeN and CuACeN), Cu addition has little effect on the intensity of CeO_2 XRD peaks. This can be attributed to the fact that a large amount of poorly dispersed crystalline CeO_2 (4.1–4.7 wt%) is already present in CeN. For the Cu/Ce/Al_2O_3 catalysts derived from the CeA (i.e. CuNCeA or CuACeA), Cu addition increases the intensity of CeO_2 XRD peaks. The effect of Cu addition on the CeO_2 peak intensity is more pronounced in the diffraction pattern of the CuNCeA catalyst compared to the CuACeA catalyst. Quantitative XRD measurements (table 1) show

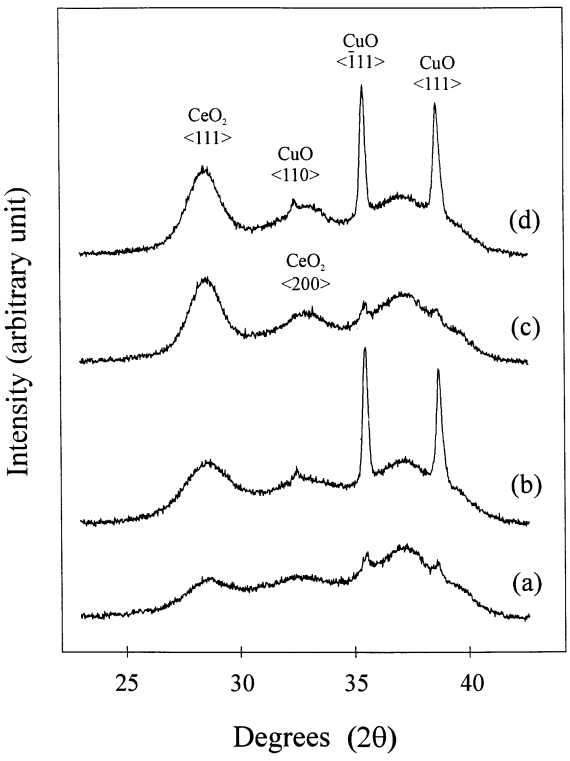

Figure 2. XRD patterns measured for (a) CuACeA, (b) CuNCeA, (c) CuACeN, and (d) CuNCeN catalysts.

that Cu addition increases the amount of crystalline CeO_2 from 0.3 wt% (CeA) to 1.5 wt% (CuACeA) and 3.4 wt% (CuNCeA). We attribute the increase in crystalline CeO_2 content observed for the CuNCeA catalyst to the dissolution of cerium oxide in an acidic copper nitrate solution (pH 2.2) followed by agglomeration during subsequent drying and calcination steps of the catalyst preparation. Cerium oxide is insoluble in the basic impregnating solution (pH 12.4) used to prepare CuA catalysts and consequently a less significant change in crystalline CeO_2 content is observed.

For the Cu/Ce/Al_2O_3 catalysts, quantitative XRD measurements show that the concentration of crystalline CuO is identical within experimental error to the value measured for analogous CuN and CuA catalysts. In addition, Ce has little effect on the Cu $2p_{3/2}$ XPS binding energies (935.0±0.1 eV). The chemical state of copper species is essentially independent of Ce promotion.

3.5. Dispersion of copper/cerium/alumina catalysts

The particle sizes of Cu and Ce species calculated using XRD line broadening and XPS intensity ratios are shown in table 2. XRD line broadening calculations show that CeO_2 particle sizes of Cu/Ce/Al_2O_3 catalysts are not changed by Cu addition and are similar to those of analogous CeN and CeA supports. However, the cerium particle size calculated from XPS Ce/Al intensity ratios increases significantly after Cu addition. Since Cu

addition increases the crystallinity of cerium oxide, we can attribute the decrease of dispersion to the agglomeration of cerium species during the Cu impregnation step. However, we cannot exclude the possibility that some copper species deposits on the surface of the cerium oxide phase, and encapsulates the particles and subsequently decreases the XPS Ce/Al intensity ratio. Such an encapsulation effect would be more prominent for copper alkoxide derived catalysts due to their higher dispersion.

The copper oxide particle sizes calculated from XRD line broadening calculations are identical regardless of cerium promotion and copper precursors. The particle sizes of copper species calculated from XPS Cu/Al intensity ratios depend on the precursors used for catalyst preparation. The absence of a significant effect of Ce addition on the CuO crystallinity and dispersion can be understood in terms of the Ce/Al_2O_3 surface structure. Since the CeN and CeA catalysts contain poorly dispersed cerium oxide, γ-Al_2O_3 is the predominant surface exposed during copper impregnation. Thus, the copper oxide structure in each catalyst is determined primarily by the copper–alumina interaction.

3.6. Effect of catalyst structure on CO oxidation activity

Table 3 shows the specific turnover frequencies (TOF) and activation energies for CO oxidation over Cu/Al_2O_3 and $Cu/Ce/Al_2O_3$ catalysts calculated at 160°C using XPS estimates of the Cu dispersion. The results of CeN and CeA catalysts are not shown due to their negligible CO oxidation activity compared to the copper catalysts. The CuN catalyst shows higher TOF and lower activation energy compared to the CuA catalyst. Comparison of the CO oxidation activities measured for the CuN and CuA catalysts indicates that the catalyst containing more crystalline CuO (i.e. CuN) is more active than catalysts containing less CuO phase (CuA). This is consistent with our previous study [53], which showed that crystalline CuO was more active for CO oxidation than a dispersed copper surface phase.

Ce addition increases the TOFs measured for the Cu/Al_2O_3 catalysts by a factor of 5 to 12. The activation energies for CO oxidation calculated for cerium promoted catalysts are similar within experimental error (12.1 ± 0.9 kcal/mol) and close to the values measured for unpromoted catalysts. The higher CO oxidation TOF for cerium promoted copper catalysts indicates that cerium oxide is an effective promoter when one considers that only a small amount of cerium oxide (5.1 wt%) was used in this study. Changing crystallinity and dispersion of cerium oxide species after Cu addition indicates that copper oxide interacts strongly with cerium oxide during catalyst preparation. Liu and Flytzani-Stephanopoulos [33,34] reported that Cu–Ce–O composite catalyst shows high CO oxidation activity, comparable to that of the Pt/alumina catalyst. They attributed the enhanced catalytic activity to the strong interaction of copper and cerium oxides. It also has been reported recently [35,36] that ceria promoter enhances the redox behavior of copper ions and produces surface oxygen ions over $CuO/CeO_2/\gamma$-alumina catalysts. The $Cu/Ce/Al_2O_3$ catalysts derived from CuN show higher CO oxidation activity than the catalyst prepared with CuA. This is consistent with the result of CuN and CuA catalysts, which shows higher CO oxidation activity for the catalyst containing more crystalline CuO.

3.7. Effect of catalyst structure on CH_4 oxidation activity

Table 3 shows the TOFs and activation energies for CH_4 oxidation calculated at 390°C. The results of CeN and CeA catalysts are not shown due to their negligible CH_4 oxidation activity compared to the copper catalysts. The TOFs of the catalysts derived from CuN are approximately three times higher than those of the catalysts prepared with CuA. Ce addition has little effect on the CH_4 oxidation TOF for copper catalysts. The activation energies are identical within experimental error (22.6 ± 0.8 kcal/mol).

We have previously reported [53] that isolated copper surface phase is the active site for CH_4 oxidation reaction over copper oxide catalyst. Therefore, the catalyst containing more isolated copper surface phase should be

Table 3
Specific turn over numbers [a] and activation energies [b] of CO and CH_4 oxidation measured for $Cu/Ce/Al_2O_3$ catalysts

Catalyst	CO oxidation		CH_4 oxidation	
	TOF ($s^{-1} \times 10^2$)	activation energy	TOF ($s^{-1} \times 10^4$)	activation energy
CuN	1.1	12.0	3.7	22.7
CuA	0.3	15.4	1.2	21.6
CuNCeN	8.7	10.9	3.7	22.7
CuACeN	3.0	12.1	1.3	23.8
CuNCeA	13.7	12.6	4.5	21.9
CuACeA	1.5	12.8	1.4	22.6

[a] Calculated at 160 and 390°C for CO and CH_4 oxidation respectively using exposed Cu species determined from XPS.
[b] Estimated from Arrhenius plots (kcal/mol) within 15% conversion.

more effective. In our study, CuA catalyst may contain less isolated copper surface phase than CuN catalyst, although Cu dispersion of CuA is higher than that of CuN. The formation of less isolated but dispersed copper phase can be attributed to the formation of Cu–DETA polymer structure during catalyst preparation step [37]. We propose that this polymeric Cu–DETA complex leads to the formation of an interacting copper surface phase (i.e. dispersed copper cluster) and/or amorphous copper oxide which may be a less active phase than isolated copper species for CH_4 oxidation. The absence of a cerium promoter effect on CH_4 oxidation reaction for $Cu/Ce/Al_2O_3$ catalysts can be explained by limited interaction between poorly dispersed cerium oxide and isolated copper surface phase.

4. Conclusions

The combined use of several techniques to investigate the effect of cerium promoter and metal precursors on the structure of $Cu/Ce/Al_2O_3$ catalysts leads to the following conclusions.

(1) The CuA catalyst shows enhanced Cu dispersion compared to CuN catalyst. However, CuA catalyst is less active for CO and CH_4 oxidation than CuN catalyst. We believe that the CuA catalyst contains less active phases than the CuN catalyst for CO and CH_4 oxidation which are crystalline CuO and isolated copper surface species, respectively.

(2) Ce has little effect on the dispersion and crystallinity of copper species. In contrast, Cu addition decreases the Ce dispersion and increases the amount of crystalline CeO_2 present in the $Cu/Ce/Al_2O_3$ catalysts, particularly in catalysts prepared using the CeA.

(3) Ce addition increases the CO oxidation activity of the copper catalysts. This can be explained by the strong interaction of cerium oxide with crystalline CuO and, subsequently, an enhancement in redox activity of the copper oxide phase. The Ce promoter does not affect CH_4 oxidation activity due to limited interaction of cerium oxide with isolated copper surface species.

Acknowledgement

Financial support from an All-University Research Initiation Grant (AURIG) administered by Michigan State University and the Center for Fundamental Materials Research (CFMR) is gratefully acknowledged.

References

[1] Y.F. Yu Yao and J.T. Kummer, J. Catal. 46 (1977) 388.
[2] J.T. Kummer, Prog. Energy Combust. Sci. 6 (1980) 177.
[3] Y.F. Yu Yao, J. Catal. 39 (1975) 104.
[4] F. Severino, J. Brito, O. Cariás and J. Laine, J. Catal. 102 (1986) 172.
[5] A.Q.M. Boon, F. van Looij and J.W. Geus, J. Mol. Catal. 75 (1992) 277.
[6] A. López Agudo, J.M. Palacios, J.L.G. Fierro, J. Laine and F. Severino, Appl. Catal. 91 (1992) 43.
[7] A.Q.M. Boon, H.M. Huisman and J.W. Geus, J. Mol. Catal. 75 (1992) 293.
[8] P. Subbanna, H. Greene and F. Desal, Environ. Sci. Technol. 22 (1988) 557.
[9] U.S. Ozkan, R.F. Kueller and E. Moctezuma, Ind. Eng. Chem. Res. 29 (1990) 1136.
[10] H. Rajesh and U.S. Ozkan, Ind. Eng. Chem. Res. 32 (1993) 1622.
[11] F. Kapteijn, S. Stegenga, N.J.J. Dekker, J.W. Bijsterbosch and J.A. Moulijn, Catal. Today 16 (1993) 273.
[12] T.-J. Huang and T.-C. Yu, Appl. Catal. 71 (1991) 275.
[13] V.N. Goetz, A. Sood and J.R. Kittrell, Ind. Eng. Chem. Prod. Res. Develop. 13 (1974) 110.
[14] R. Prasad, L.A. Kennedy and E. Ruckenstein, Catal. Rev. Sci. Eng. 26 (1984) 1.
[15] C.J. Heyes, J.G. Irwin, H.A. Johnson and R.L. Moss, J. Chem. Tech. Biotechnol. 32 (1982) 1025.
[16] Y.F. Yu Yao and J.T. Kummer, J. Catal. 106 (1987) 307.
[17] E.C. Su, C.N. Montreuil and W.G. Rothschild, Appl. Catal. 17 (1985) 75.
[18] H.S. Gandhi, A.G. Piken, M. Shelef and R.G. Delosh, SAE paper No. 760201 (1976).
[19] R. Dictor and S. Roberts, J. Phys. Chem. 93 (1989) 5846.
[20] F. Le Normand, L. Hilaire, K. Kili, G. Krill and G. Maire, J. Phys. Chem. 92 (1988) 2561.
[21] G. Kim, Ind. Eng. Chem. Prod. Res. Dev. 21 (1982) 267.
[22] R.K. Herz and J.A. Sell, J. Catal. 94 (1985) 166.
[23] S.H. Oh, J. Catal. 124 (1990) 477.
[24] Y.F. Yu Yao, J. Catal. 87 (1984) 152.
[25] S.H. Oh and C.C. Eickel, J. Catal. 112 (1988) 543.
[26] H.C. Yao and Y.F. Yu Yao, J. Catal. 86 (1984) 254.
[27] R.K. Herz, Am. Chem. Soc. Symp. Ser. 178 (1982) 59.
[28] T. Jin, T. Okuhara, G.J. Mains and J.M. White, J. Phys. Chem. 91 (1987) 3310.
[29] B.K. Cho, B.H. Shanks and J.E. Bailey, J. Catal. 115 (1989) 486.
[30] S.K. Agarwal, J.J. Spivey and J.B. Butt, Appl. Catal. 81 (1992) 239.
[31] R.E. Bedford and W.J. LaBarge, US Patent 5,063,193 (1991).
[32] W. Liu, A.F. Sarofim and M. Flytzani-Stephanopoulos, Appl. Catal. B 4 (1994) 167.
[33] W. Liu and M. Flytzani-Stephanopoulos, J. Catal. 153 (1995) 304.
[34] W. Liu and M. Flytzani-Stephanopoulos, J. Catal. 153 (1995) 317.
[35] G. Lu and R. Wang, Cuihua Xuebao 12 (1991) 314.
[36] Y. Tian, Y. Fu and P. Lin, Cuihua Xuebao 15 (1994) 189.
[37] F. Uchikawa and J.D. Mackenzie, J. Mater. Res. 4 (1989) 787.
[38] *Powder Diffraction File: Inorganic Phases*, Joint Committee on Powder Diffraction Standards, PA, 1983.
[39] H.P. Klug and L.E. Alexander, *X-Ray Diffraction Procedures for Polycrystalline and Amorphous Materials*, 1st Ed. (Wiley, New York, 1954).
[40] B.R. Strohmeier, D.E. Leyden, R.S. Field and D.M. Hercules, J. Catal. 94 (1985) 514.
[41] B. Wallbank, C.E. Johnson and I.G. Main, J. Electron. Spectrosc. Relat. Phenom. 4 (1974) 263.
[42] A. Rosencwaig and G.K. Wertheim, J. Electron. Spectrosc. Relat. Phenom. 1 (1972) 493.
[43] Z.T. Al-Dhhan, T. Hashemi and C.A. Hogarth, Spectrochim. Acta 44b (1989) 205.
[44] E. Paparazzo, Surf. Sci. 234 (1990) L253.

[45] E. Paparazzo, G.M. Ingo and N. Zacchetti, J. Vac. Sci. Technol. A 9 (1991) 1416.
[46] P.W. Park and J.S. Ledford, Langmuir 12 (1996) 1794.
[47] C. Deffosse, D. Canesson, P.G. Rouxhet and B. Delmon, J. Catal. 51 (1978) 269.
[48] F.P.J.M. Kerkhof and J.A. Moulijn, J. Phys. Chem. 83 (1979) 1612.
[49] J.H. Scofield, J. Electron. Spectrosc. Relat. Phenom. 8 (1976) 129.
[50] D.R. Penn, J. Electron. Spectrosc. Relat. Phenom. 9 (1976) 29.
[51] J.Z. Shyu, W.H. Weber and H.S. Gandhi, J. Phys. Chem. 92 (1988) 4964.
[52] R.M. Friedman, J.J. Freeman and F.W. Lytle, J. Catal. 55 (1978) 10.
[53] P.W. Park and J.S. Ledford, Appl. Catal. B, in press.